THE JOURNAL OF PHYSICAL CHEMISTRY B

Article

Cite This: J. Phys. Chem. B 2019, 123, 9272−9280

pubs.acs.org/JPCB

Complex Self-Assembly from Simple Interaction Rules in Model Colloidal Mixtures

Santi Prestipino,*[,†] Domenico Gazzillo,[‡] Gianmarco Munaò,[†] and Dino Costa[†]

[†]Dipartimento di Scienze Matematiche e Informatiche, Scienze Fisiche e Scienze della Terra, Università degli Studi di Messina, Viale F. Stagno d'Alcontres 31, 98166 Messina, Italy

[‡]Dipartimento di Scienze Molecolari e Nanosistemi, Università di Venezia "Ca' Foscari", Via Torino 155, 30172 Venezia Mestre, Italy

ABSTRACT: Building structures with hierarchical order through the self-assembly of smaller blocks is not only a prerogative of nature, but also a strategy to design artificial materials with tailored functions. We explore in simulation the spontaneous assembly of colloidal particles into extended structures, using spheres and size-asymmetric dimers as solute particles, while treating the solvent implicitly. Besides rigid cores for all particles, we assume an effective short-range attraction between spheres and small monomers to promote, through elementary rules, dimer-mediated aggregation of spheres. Starting from a completely disordered configuration, we follow the evolution of the system at low temperature and density, as a function of the relative concentration of the two species. When spheres and large monomers are of same size, we observe the onset of elongated aggregates of spheres, either disconnected or cross-linked, and a crystalline bilayer. As spheres grow bigger, the self-assembling scenario changes, getting richer overall, with the addition of flexible membrane sheets with crystalline order and monolayer vesicles. With this wide assortment of structures, our model can serve as a viable template to achieve a better control of self-assembly in dilute suspensions of microsized particles.

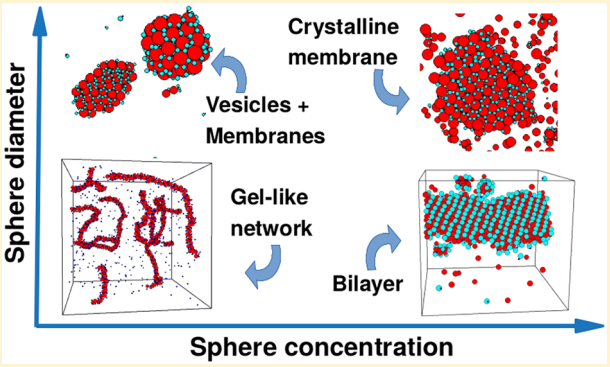

1. INTRODUCTION

Various biomolecules, like phospholipids, peptides, and DNA filaments, as well as many synthesized colloidal particles have the capability of assembling into mesophases as a result of their chemical and structural versatility (see, e.g., ref 1). The spontaneous assembly of colloidal particles into extended structures, like gels or membranes, is an emergent phenomenon of utmost importance in the design of functional materials. One motif that may serve different purposes is a colloidal sphere endowed with one or more attractive caps, so-called "patches", obtained by grafting appropriate functional groups to the sphere surface—see the examples in refs 2−5. When assembled in a connected network characterized by a high surface-to-volume ratio, patchy particles may provide a practical morphology for nanoporous catalysts.[6] At lower densities, Janus particles form micelles and even small bilayer shells.[7] Surfactants, i.e., molecules with amphiphilic character, are another class of substances that produce micelles in water. By forming micelles, surfactant molecules avoid the contact of their hydrophobic groups with water, thereby minimizing distortion of the hydrogen-bonding network. Surfactants may also self-assemble into vesicles (closed bilayers).[8] Recently there has been growing interest in vesicles because of their wide application in biology and medicine as model cell membranes and for their potential as drug carriers and encapsulating agents.[9−11] Vesicles can also be shaped with lipids ("liposomes") and block copolymers ("polymersomes").[12] Whether micelles or vesicles are formed depends on a subtle balance between entropy and energy. While entropy always favors spherical micelles, energetic/packing considerations put restrictions on the size and shape of aggregates: single-chain amphiphiles tend to form globular or rodlike micelles, whereas double-chain molecules prefer to make bilayers.[13] Naturally, crystallization is a simpler form of self-assembly. A large variety of complex crystals and quasicrystals have recently been obtained using particles with anisotropic shape[14] or isotropic interactions featuring multiple potential wells.[15] The wealth of supramolecular structures in materials with directional interactions provides the original motivation for seeking theoretical models that can be employed for a bottom-up description of these systems.

Our challenge is to obtain complex phase behavior with minimal assumptions about the interparticle forces, possibly without modifying the interaction laws in response to a change in the target structure. In this respect, we have recently ascertained the usefulness of size-asymmetric dimers as

Received: September 10, 2019
Revised: October 4, 2019
Published: October 4, 2019

DOI: 10.1021/acs.jpcb.9b08617
J. Phys. Chem. B 2019, 123, 9272−9280

encapsulating agents for spherical particles in a colloidal-poor solution.[16,17] Inspired by those findings, in this paper we provide a systematic study of aggregation in model colloidal mixtures of spheres and dimers. A rich self-assembly diagram emerges in the low-density regime, which counts many diverse aggregates as a function of concentration and size unbalance between the species—including a gel-like network, a crystalline bilayer, various shapes of crystalline membranes, and spheroidal vesicles.

2. MODEL AND METHOD

Within an implicit-solvent scheme, we consider a dispersion of two colloidal species: a sphere (A) and a dimer made up of two tangent spherical monomers (B), in which one end (B_1) is 3 times smaller than the other (B_2). Particle A is represented as a hard sphere of diameter $\sigma_A = d\sigma_{B_2}$ with d = 1, 2, or 3 in this work. All particle interactions are hard-core with additive diameters $\sigma_{\alpha\beta} = (\sigma_\alpha + \sigma_\beta)/2$, except for the A−$B_1$ interaction, which is given by a hard-core plus square-well potential:

$$u(r) = \begin{cases} \infty & \text{for } r < \sigma_{AB_1} \\ -\epsilon & \text{for } \sigma_{AB_1} \le r \le \sigma_{AB_1} + \sigma_{B_1} \\ 0 & \text{otherwise} \end{cases} \quad (1)$$

With such interaction rules, at low density and temperature spheres get coated with dimers. The rather strong asymmetry in size between B_1 and B_2 ensures more effective encapsulation of spheres by dimers. No mutual attraction is assumed between two dimers or between two spheres, with the idea that such interactions (which are usually present in real colloids[18]) are much weaker than ϵ. In this way we keep the system as simple as possible in order to identify the minimal ingredients for a fairly complex self-assembly diagram. The size difference between A and B_2, expressed by the ratio of their diameters, d, is the only free parameter left in the model. We take σ_{B_2} and ϵ as units of length and energy, respectively, and in turn define a reduced distance $r^* = r/\sigma_{B_2}$ and a reduced temperature $T^* = k_B T/\epsilon$, where k_B is the Boltzmann constant; hereafter, reduced units are assumed, and the asterisks are omitted altogether. Finally, we denote by N_A and N_B the numbers of spheres and dimers, respectively. Hence $N = N_A + N_B$ is the total number of particles and $\chi = N_A/N$ is the concentration of spheres.

We performed Monte Carlo (MC) simulations of the A−B mixture in the canonical ensemble using the standard Metropolis algorithm with periodic conditions at the boundaries of a cubic box. Canonical conditions mimic the natural setting of a mixture of spheres and dimers where the number of particles of each species and the volume of the container are fixed. One MC cycle consists of N Metropolis moves. For dimers, one trial move was a random choice between a center-of-mass translation and a rotation about a coordinate axis. The maximum shift and rotation were adjusted during the first part of the run so that the ratio of accepted to total number of moves stayed close to 60%. The acceptance rule and the schedule of the moves were designed to satisfy detailed balance.

We started each simulation run from a random configuration of the system to simulate its thermalization after a quench from high temperature (we generated runs of 3−7 billion MC cycles). The relative amount of A and B was adjusted to the prescribed concentration of spheres, χ; the temperature was T = 0.15, and the density ρ was at most 0.05. We summarize in Table 1 the conditions assumed in our runs. Four distinct runs were performed for d = 2 and χ = 0.20 as well as for each case relative to d = 3 and χ = 0.20 in order to collect more statistics for the all-important case of self-assembly into crystalline membranes and vesicles. In the latter case, we doubled the number of particles also to rule out any possible size dependence of the self-assembly results. The temperature of 0.15 is a compromise: it is sufficiently small to observe long-lasting aggregates but still high enough to allow for escape from shallow energy minima.

Table 1. Thermodynamic Conditions Adopted during the Simulations, All Performed for T = 0.15

d	χ	N_A	N_B	ρ	η_A	no. of runs
1	0.10	200	1800	0.05	0.002618	1
1	0.20	400	1600	0.05	0.005236	1
1	1/3	400	800	0.05	0.008727	1
1	0.50	400	400	0.05	0.013990	1
2	0.10	100	900	0.032	0.01340	1
2	0.20	200	800	0.016	0.01340	4
2	1/3	333	667	0.0096	0.01340	1
2	0.40	400	600	0.008	0.01340	1
2	0.50	400	400	0.0064	0.01340	1
3	0.10	100	900	0.01	0.01414	1
3	0.20	200	800	0.005	0.01414	4
3	0.20	400	1600	0.005	0.01414	4
3	0.20	400	1600	0.0025	0.00707	4
3	1/3	333	667	0.003	0.01414	1
3	0.40	400	600	0.0025	0.01414	1
3	0.50	400	400	0.002	0.01414	1

In the production runs, which were typically 2×10^8 cycles long, we computed various radial distribution functions (RDFs). Even in a strongly heterogeneous system, the sphere−sphere RDF $g_{AA}(r)$ bears valuable information on the arrangement of spheres in a close neighborhood of a reference sphere. Useful indications about the relative separation of spheres and dimers were instead obtained from $g_{AB_1}(r)$.

The fractal dimension of the subsystem of spheres can be obtained from $g_{AA}(r)$: choosing a sphere as the reference, for each fixed radius R one counts the number of spheres within a distance R from the reference sphere and then averages over all of the spheres. The outcome is the "mass" M of the sphere backbone as a function of R. Typically, $M(R) \sim R^D$ at large R, which defines D as the *mass fractal dimension* of the spheres. It follows immediately from the definition of the sphere−sphere RDF that

$$M(R) = 4\pi\rho\chi \int_0^R \mathrm{d}r\, r^2 g_{AA}(r) \quad (2)$$

which allows one to readily obtain D from $g_{AA}(r)$.

To gain better insight into the system structure, we carried out a cluster analysis by identifying at regular times, and counting as a function of size, assemblies of connected spheres by the Hoshen−Kopelman algorithm.[19] Two spheres are connected if their distance is smaller than $r_{min} = \sigma_A + 3\sigma_{B_1} = (d + 1)\sigma_{B_2}$, which represents the maximum distance at which two spheres can still be "in contact" through a B_1 monomer placed in the middle. Finally, the cluster size distribution (over a fixed time interval) is defined as

DOI: 10.1021/acs.jpcb.9b08617
J. Phys. Chem. B 2019, 123, 9272−9280

$$\mathcal{N}(n) = \frac{nN_{cl}(n)}{N_A} \tag{3}$$

where $N_{cl}(n)$ is the average number of n-sized clusters per system configuration. The distribution (S2) is so normalized that $\sum_n \mathcal{N}(n) = 1$.

3. RESULTS AND DISCUSSION

Simulations were kept going until the total potential energy U fluctuated around a constant value for a long time (a few billion cycles), signaling that a (meta)stable equilibrium had been reached at last. In Figure 1, we report some representative

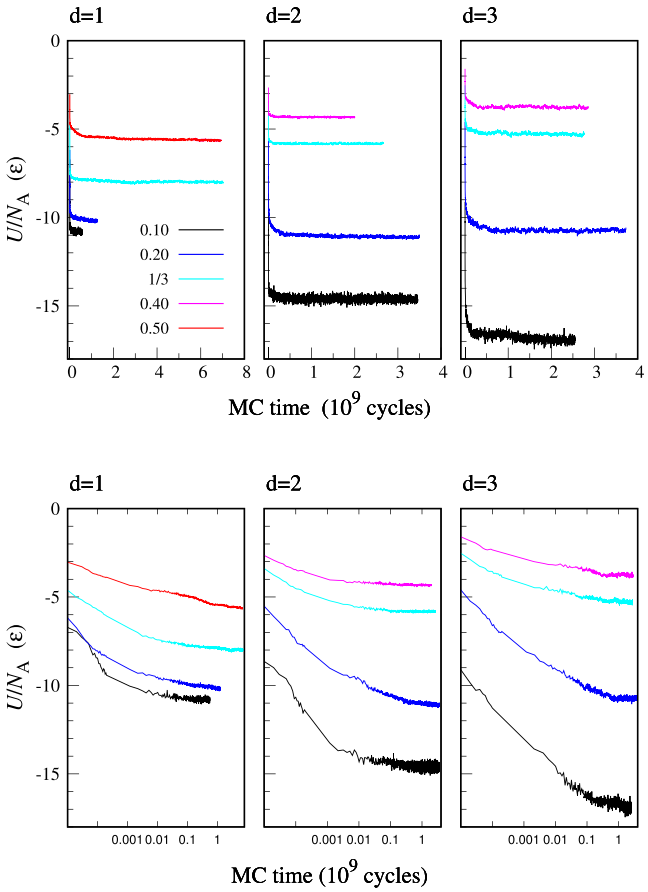

Figure 1. MC evolution of the potential energy per sphere for a few d and χ values (see the legend). (top) Standard linear scale. (bottom) Semilog scale.

cases of U evolution in the course of simulation. Each curve refers to an individual run, i.e., no average was made over several runs performed under identical conditions. As evidenced by a glance at the configuration of the system at regular intervals, relaxation initially proceeds through the progressive accretion of a few sphere aggregates, glued together by dimers, which is reflected in a rapid (exponential) decay of U. Subsequently, U decreases more slowly as clusters begin to coalesce, until it levels off after $\sim 10^9$ cycles. A slowdown of relaxation (aging) also occurs for large χ (>0.50), where the formation of extended sphere aggregates is hampered by the shortage of dimers. Any coagulation event is manifested in a tiny downward jump in U as a function of time; however, since the joining of clusters is a relatively rare event, at least on the time scale of single-particle diffusion, the decrease in U is slower in the later stages of the evolution than in the first stages. On the other hand, a well-defined drop in U as a function of MC time signals an extensive rearrangement of the structure, as clearly seen for $d = 3$ and $\chi = 0.10$ (black lines in the right panels of Figure 1).

As aggregates grow in size and relax, the dimers on the surface become increasingly effective in screening the aggregate from the outside particles. Indeed, a growing aggregate gets progressively covered with the inert B_2 particles, while the "reactive" particles (i.e., B_1 monomers and spheres) lie buried within. The next step in equilibration is cluster coalescence, a.k.a. coarsening/Ostwald ripening, which for $T = 0.15$ typically starts 10^7-10^8 cycles after the initial quench. When two clusters meet, they usually stick together to form a bigger aggregate. The kinetics of coarsening is strongly influenced by the system density, i.e., by the crowding around the aggregates, which affects the rate of collisions and indirectly the type of frozen architectures arising at low temperature. Unless the initial concentration of spheres is very low, a unique aggregate encompassing all of the spheres in the system eventually appears, as witnessed by the MC evolution of the maximum cluster size in the left panel of Figure 2. Details are provided in

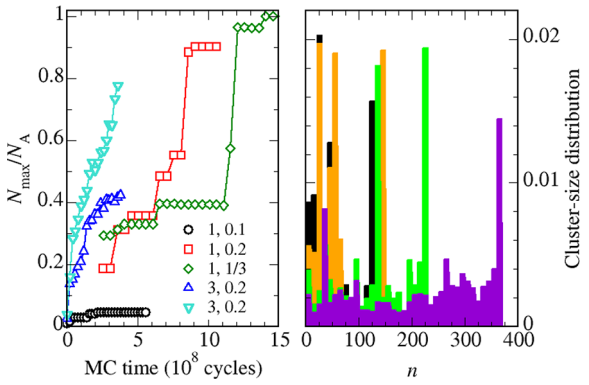

Figure 2. (left) Size of the maximum cluster of spheres, N_{max}, computed at discrete times along the MC trajectory for $N_A = 400$ and a few combinations of d and χ (see the legend). The data for $d = 1$ refer to $\rho = 0.05$; the data for $d = 3$ are averages over four distinct runs (upward triangles, $\rho = 0.0025$; downward triangles, $\rho = 0.005$). (right) Cluster size distribution for $d = 1$ and $\chi = 0.20$, as computed over four distinct intervals of 10^8 cycles separated by 2×10^8 cycles (temporal sequence: black, orange, green, purple).

the right panel, where we show how the cluster size distribution evolves in a single run for $d = 1$ and $\chi = 0.20$: as coarsening proceeds, the weight of small sizes is progressively reduced in favor of the maximum cluster size until a unique peak centered at the total number of spheres N_A (400 in this figure) is left over.

We sum up our findings in the (χ, d) diagram shown in Figure 3, which yields a bird's eye view of the self-assembled structures developed in the system at low density and temperature. In the following, we separately discuss results for $d = 1$ and $d = 2$, 3 in subsections 3.1 and 3.2, respectively. Finally, in subsection 3.3 we show by analytic arguments that the nature of self-assembly for $d = 1$ is necessarily different from that for $d = 2$ or 3.

3.1. $d = 1$. For $d = 1$ we set the density at 0.05 and consider χ values from 0.10 to 0.50. For $\chi = 0.10$ we observe a homogeneous distribution of small clusters of spheres coated with dimers ("micelles"—see Figure 3a). We see in the left

DOI: 10.1021/acs.jpcb.9b08617
J. Phys. Chem. B 2019, 123, 9272−9280

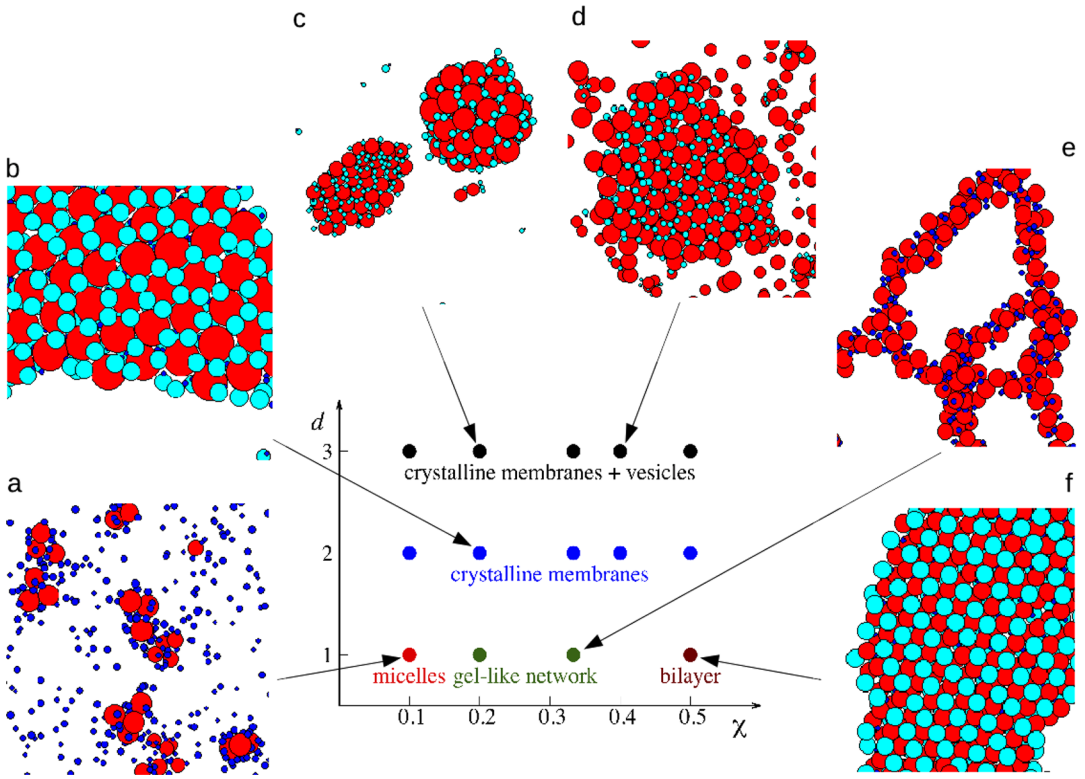

Figure 3. Schematic diagram of self-assembly at low density (circles denote the state points where simulations were carried out). For selected (χ, d) pairs, we show the typical structure of the system at equilibrium (spheres are in red; B_1 and B_2 monomers are in blue and cyan, respectively). Only a portion of the system is depicted in the snapshots. In (a) and (e), B_2 particles have been omitted for clarity.

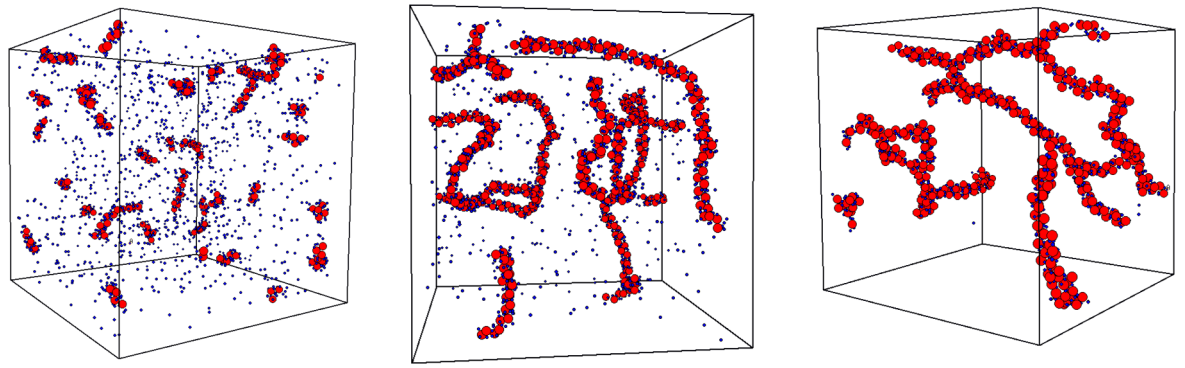

Figure 4. Aggregates for d = 1: micelles (χ = 0.10, left) and gel-like networks (χ = 0.20, middle; χ = 1/3, right). B_2 particles are hidden for a better visualization of the sphere backbone.

panel of Figure 4 that both spherical and rodlike micelles are formed. The dimers around the spheres, exposing B_2 monomers outside, are so tight together that they prevent coalescence of clusters. Therefore, aggregation of spheres is successfully contrasted. In a similar way, stabilization of polystyrene microspheres by dumbbell-shaped colloids with a sticky lobe and a nonsticky lobe was demonstrated in ref 18.

Clearly, micellization is only stable provided that the concentration χ is low enough, and this is apparently the case for χ = 0.10. For higher concentrations, spheres eventually become part of a unique aggregate whose nature depends on χ. For χ = 0.20 and χ = 1/3, a percolating network is formed (see Figure 3e and the middle and right panels of Figure 4). Indeed, spheres are now numerous enough to rule out the occurrence of spherical micelles, opening the way to the formation of long chains of spheres. Each sphere along the chain binds 8−10 dimers (depending on χ) to be shared with its neighboring spheres, as witnessed by the energy level in Figure 1 (left panels). Indeed, the absolute value of U/N_A is the mean number of B_1 monomers bound to a sphere. Close scrutiny of the chains for χ = 0.20 reveals a zigzag structure (Figure 5, left), a motif that is also present in rodlike micelles for χ = 0.10. For χ = 1/3, the chain geometry with the most effective combination of low energy and high entropy is given by three helicoidal strands of spheres wrapped around a common (curved) axis (Figure 5, right). During the MC evolution, the presence of unsaturated bonds on the chain surface makes crossing/branching of chains a likely outcome, eventually resulting in a connected network that percolates throughout the simulation box. Once this spanning network has been established (which takes ~10^9 MC cycles for T = 0.15), no further rearrangement occurs at the large scale: the aggregate

DOI: 10.1021/acs.jpcb.9b08617
J. Phys. Chem. B 2019, 123, 9272−9280

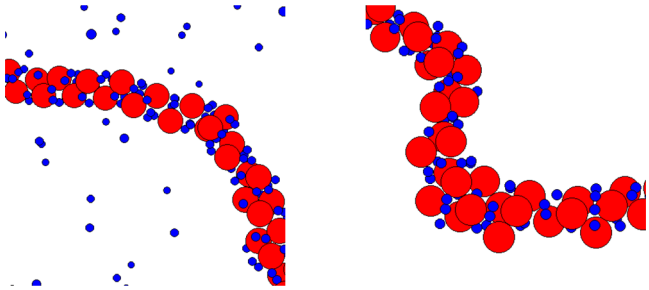

Figure 5. Chain details of gel-like networks for $d = 1$: (left) $\chi = 0.20$; (right) $\chi = 1/3$. B_2 particles are not shown.

has become a gel. We computed the mass fractal dimension of the backbone of connected spheres and found it to be close to 1.8, seemingly at odds with the intuition that a chain network is a one-dimensional manifold. In fact, a fractal dimension between 1 and 2 is a reasonable outcome considering that chains have a nonvanishing thickness and that because of the high number of nodes in the network a relevant fraction of spheres are not located in the body of a chain.

Looking at the distribution of the angle α between two A−A bonds with one sphere in common at the angle vertex, we see a resemblance between the distributions for $\chi = 0.10$ and $\chi = 0.20$ (compare the circles and squares in the left panel of Figure 6), which can be ascribed to the similarity between the

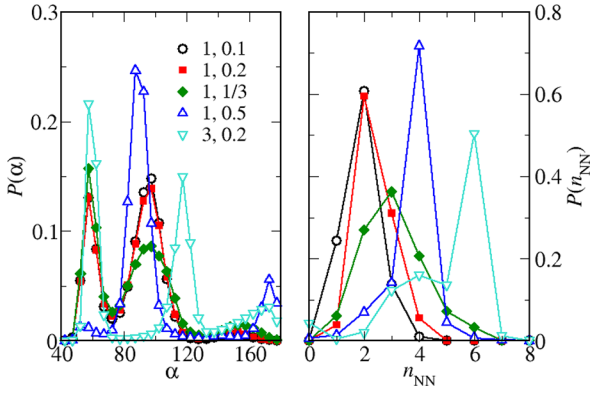

Figure 6. (left) Distributions of the angle α formed by two A−A bonds sharing one sphere at the angle vertex for a few combinations of d and χ (see the legend). The data for $d = 1$ and $d = 3$ refer to $\rho = 0.05$ and 0.0025, respectively. (right) Distributions of the number of spheres that are nearest neighbors to a given sphere, n_{NN}.

local structures of rodlike micelles and gels. In detail, while the peak centered at 60° points to the existence of a high number of triplets of spheres in reciprocal contact, the broader peak around 100° indicates a preference for local cubic and tetrahedral orderings as well as for zigzag order with this characteristic angle. Upon going from $\chi = 0.10$ to $\chi = 1/3$, the mean number of spheres that are nearest neighbors to a reference sphere, n_{NN}, grows from $\lesssim 2$ to $\gtrsim 3$ (Figure 6, right).

With a further increase in concentration, the geometry of self-assembly changes again: for $\chi = 0.50$ we see the onset of a crystalline bilayer that grows laterally through the inclusion of spheres and dimers from the solution (Figures 3f and 7). The arrangement of particles in the bilayer is very peculiar: each layer of spheres forms a rectangular crystal displaced by half of the lattice spacing relative to the other layer; B_1 particles occupy the interstices between the spheres, so that each sphere

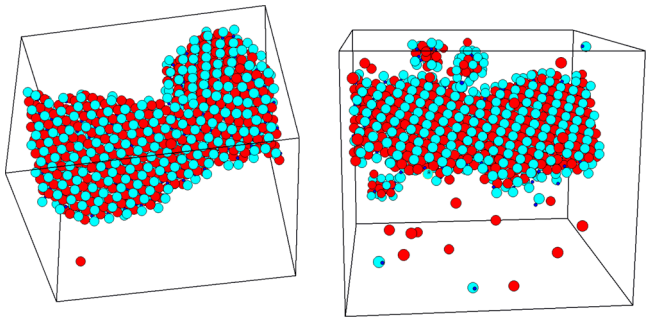

Figure 7. Crystalline bilayers ($d = 1, \chi = 0.50$): (left) $T = 0.15$; (right) $T = 0.20$.

is bound to exactly six dimers (see the details in subsection 3.3). This structure is reflected in the α distribution (Figure 6, left), which shows a distinct peak at 90°, and in the n_{NN} distribution, which is peaked at 4 (Figure 6, right). The mass fractal dimension is now about 2.1, consistent with the idea that a bilayer is essentially two-dimensional. When the system is heated from $T = 0.15$ to $T = 0.20$, we find that the bilayer structure remains stable, even though small clusters of spheres and dimers detach from the bilayer edge to reach the solution (Figure 7, right).

We also investigated the spatial distribution of spheres at a local level using RDFs (see Figure 8), which confirmed the structural similarity between $\chi = 0.10$ and $\chi = 0.20$. With increasing concentration, the maximum of $g_{AA}(r)$ at contact is progressively reduced as the system departs more and more from micelles. In the range $\chi = 0.10$ to 1/3, the second peak is associated with bound pairs of spheres separated by a B_1 particle. We see that it broadens until for $\chi = 0.50$ it splits in two (we comment more on this point in subsection 3.3).

3.2. $d = 2, 3$. The value of d is rather crucial for the stability of the crystalline bilayer, which no longer exists for d larger than ∼1.35 (see the theoretical argument in subsection 3.3). Indeed, for $d = 2$ or 3 the nature of the self-organized structures is different. Aggregates are now monolayer sheets over the whole χ range from 0.10 to 0.50, made up of sixfold-coordinated spheres held together by dimers ("crystalline membranes", often resulting from the fusion of smaller patches), as shown in Figure 3b−d: each sphere is bound to 12 dimers on average (six on each face of the sheet), located in the interstices between triplets of neighboring spheres. The finite range of attraction allows for some tolerance in the separation between spheres and in the position of intercalated dimers; as a result, membranes are not perfectly flat but can bend to a certain extent. Crystalline membranes usually coexist with a sizable number of isolated dimers ($\chi < 0.20$) or spheres ($\chi > 0.20$). Only for $\chi = 0.20$ is the right proportion of spheres and dimers reached for building lamellar aggregates without excess particles. In subsection 3.3 we provide a theoretical argument ruling out the existence of membranes for $d = 1$.

The rich catalog of membrane morphologies can be appreciated in Figure 9, which is relative to $d = 2$. For $\chi = 0.10$ the observed aggregates are one-layer sheets with holes (left). When the concentration is increased to 0.20, more conventional membranes are observed (middle), which are flat or only slightly curved. Occasionally, more exotic structures are seen: an example of a twisted crystalline membrane that gives an atomistic representation of a Möbius strip is shown in the right panel of Figure 9.

DOI: 10.1021/acs.jpcb.9b08617
J. Phys. Chem. B 2019, 123, 9272−9280

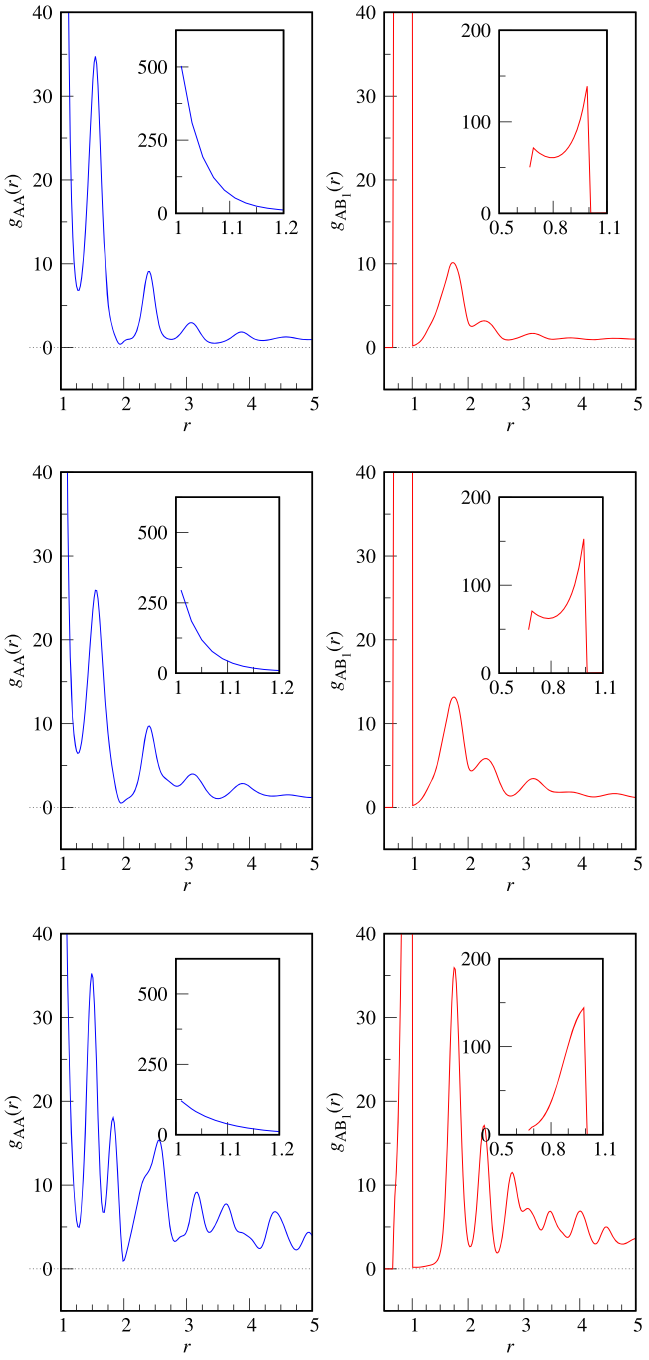

Figure 8. The RDFs $g_{AA}(r)$ (left) and $g_{AB_1}(r)$ (right) for $d = 1$ and $\rho = 0.05$. From top to bottom, curves refer to $\chi = 0.10$, 0.20, and 0.50. Magnifications of the contact regions are reported in the insets.

The triangular array of spheres within membranes has clear imprints in the structural indicators. This is evidenced in the narrow peak at 60° in the α distribution (Figure 6, left), with replicas at 120° and 180°, as well as in the maximum at 6 in the n_{NN} distribution (Figure 6, right). The triangular order is also revealed in the locations of the first few peaks in the sphere−sphere RDF (Figure 10): indeed, for $d = 3$ and $\chi = 0.20$ we see that the first three shell radii of the triangular lattice all occur in the profile of $g_{AA}(r)$, whereas the first peak of $g_{AB_1}(r)$ corresponds to B_1 particles located in the interstices between triplets of neighboring spheres.

Looking back at Figure 1, we can now explain that the different d dependences of the asymptotic value of U for fixed χ are due to the diversity of self-assembly solutions devised by the system as a function of d. For $\chi = 0.10$ there is no preferential site for binding of dimers to a sphere, and therefore, the asymptotic value of $|U|/N_A$ is an increasing function of d for the simple reason that a bigger sphere can bind a larger number of dimers. On the contrary, for $\chi = 1/3$ or 0.50 the decrease in $|U|/N_A$ with d just demonstrates the higher efficiency of spheres to bind dimers for $d = 1$, where a gel-like network ($|U|/N_A = 8-10$) or a crystalline bilayer ($|U|/N_A = 6$) occurs. For $d = 2$ or 3, one might expect that $U/N_A \approx -12$ (since this is the specific energy in a crystalline membrane); however, for $\chi > 0.20$ membranes are floating in a background of unbound spheres, and this pushes the asymptotic value of U/N_A upward relative to −12, the more so the larger χ is relative to 0.20.

The spontaneous generation of flexible membranes is an attractive feature of our mixture, since it brings about the possibility of vesicle formation from scratch (at least under high-dilution conditions). Vesicles have long been recognized as a fundamental requisite of life,[20] since all known life forms are cellular and each cell is screened from the environment by a closed bilayer shell composed of lipids and proteins in a fluid state. Molecular simulations[21−26] and small-angle X-ray scattering experiments[27] have shown that vesiculation of amphiphiles usually proceeds from small discoidal patches that beyond a certain size are energetically preferred to spheroidal grains. Gradually, these patches grow by joining of individual amphiphiles to the peripheral contour. To reduce the contour energy, a sufficiently large patch acquires a definite curvature until it eventually folds into a vesicle.[28,29] Notably, in our model the onset of vesicles follows the same path but for the difference that membrane sheets are now crystalline and single-layer (see Figure 11, left). Clearly, the decrease in contour energy during the transition from a planar sheet to a vesicle is hampered by an increase in bending energy due to stretching of bonds, leading ultimately to the existence of a minimum membrane radius below which the formation of vesicles is unfavorable.[13,30] Crystalline membranes can circumvent this limitation by the proper insertion of a few fivefold disclinations, relieving the strain associated with the defect by buckling out of the plane.[31−36] The same mechanism is at work in our model, where the appearance of disclinations at suitable locations makes a small membrane sheet able to transform into a vesicle (Figure 11, middle). Around each conical protrusion, several facets merge together to form a cup-shaped intermediate stage in vesicle development. A similar process occurs in small spherical crystals of hard particles,[37−40] where the gathering of disclinations at the vertices of an icosahedron (i.e., at the maximum possible relative distance) guarantees the largest possible entropy, i.e., the highest number of sixfold particles. For $d = 2$, membrane sheets appear to be flatter (i.e., stiffer) compared with $d = 3$. This is due to a stronger mutual obstruction of nearby B_2 monomers in curved membranes (see the details in subsection 3.3); as a result, in small system samples the propensity of membranes to evolve into vesicles is smaller for $d = 2$ than for $d = 3$.

We have already mentioned the importance of vesicles as "containers" of molecules of fundamental importance for life. This strongly depends on the lipid vesicle being impenetrable to most solutes. Interestingly, because of the occupation of

DOI: 10.1021/acs.jpcb.9b08617
J. Phys. Chem. B 2019, 123, 9272−9280

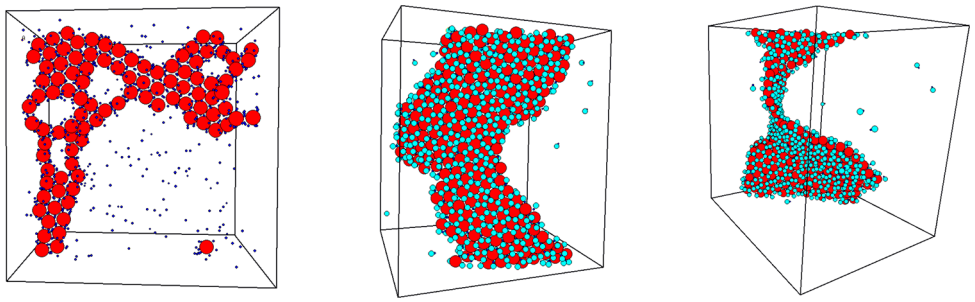

Figure 9. (left) Membrane with holes (d = 2 and χ = 0.10; B_2 particles are not shown). (middle) A more conventional membrane for d = 2, χ = 0.20, and ρ = 0.016. (right) Möbius strip (χ = 0.20 and ρ = 0.016).

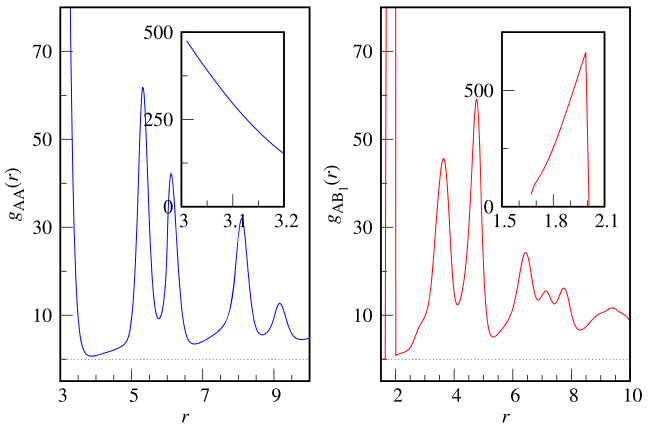

Figure 10. RDFs $g_{AA}(r)$ (left) and $g_{AB_1}(r)$ (right) for d = 3, χ = 0.20, and ρ = 0.0025. Magnifications of the contact regions are reported in the insets.

sphere interstices by dimers, also our colloidal vesicles are impermeable, making encapsulation effective.

It seems inevitable for any sufficiently flexible membrane sheet in our model to eventually form a vesicle. However, during the simulation run two aggregates may occasionally collide and join together. In particular, a forming vesicle may encounter another aggregate on its path and then vesiculation gets arrested. Clearly, a vesicle can arise as an individual entity only if the characteristic time for a membrane to fold and close is shorter than the average collision time. In this regard, in the right panel of Figure 11 we note the simultaneous occurrence of two vesicles, one of which is bound to a curved membrane. While the presence of two vesicles in a small sample is to be regarded as an exceptional event, it is confirmed that in our system the natural tendency of membrane sheets is to fold into vesicles.

3.3. Stability of Crystalline Structures. In this subsection we prove (*i*) that the crystalline bilayer found for d = 1 and χ = 0.50 cannot survive above $d \approx 1.35$ and conversely (*ii*) that a triangularly ordered sheet (i.e., a flat membrane of infinite size) cannot exist for d smaller than ∼1.5.

3.3.1. Bilayer. Looking closely at the configuration pictured in the left panel of Figure 7, relative to d = 1 and χ = 0.50, we see that spheres are arranged in two rectangular layers with lattice spacings a and b (with $a > b$), displaced by c in the third direction. Dimers are oriented perpendicular to the layers, such that the B_1 monomers are nested in the interstices of each layer whereas the B_2 monomers are exposed to the outside. In a convenient reference system, the coordinates of spheres in the bottom layer are $(ai, bj, 0)$ with $i, j = 0, \pm1, \pm2, ...$, while those of spheres in the top layer are $(ai + a/2, bj, c)$. In turn, the B_1 particles in the bottom layer have coordinates $(a/2 + ai, b/2 + bj, 0)$, whereas those in the top layer are located at $(ai, b/2 + bj, c)$. Hence, the four B_1 particles that are in-plane neighbors of a given sphere are at a distance of $d_{in} = \sqrt{a^2 + b^2}/2$, while the two B_1 particles that are out-of-plane neighbors of a sphere are a distance $d_{out} = \sqrt{b^2 + 4c^2}/2$ apart. Instead, the distance between two closest spheres lying in different layers is $d_{ss} = \sqrt{a^2 + 4c^2}/2$. For symmetry reasons it must be true that $d_{in} = d_{out}$, which implies that $c = a/2$ and $d_{ss} = a/\sqrt{2}$. Both d_{ss} and b should be larger than σ_A = 1, which implies that $a \geq \sqrt{2}$, $b \geq 1$, and $c \geq \sqrt{2}/2$. When all of the equal signs apply, $d_{in} = d_{out} = \sqrt{3}/2$. In order to have a bond between a sphere and a dimer, the relative distance between A and B_1

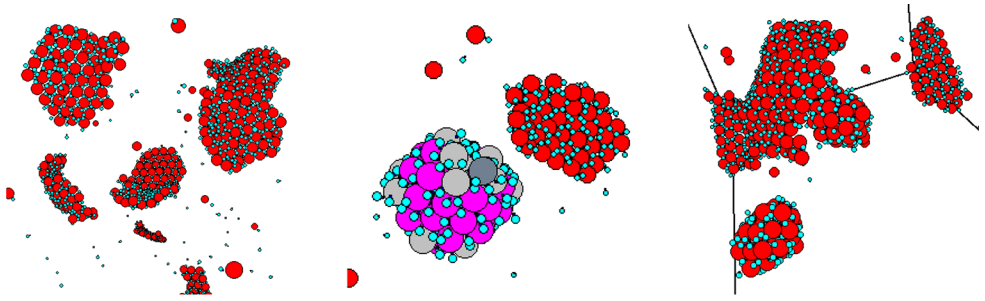

Figure 11. (left) Typical configuration of the A−B mixture for d = 3, χ = 0.20, and ρ = 0.0025. (middle) Vesicle with a membrane in the background. In the vesicle, fourfold, fivefold, and sixfold spheres (46 in total) are colored in slate gray, light gray, and magenta, respectively. (right) Lamellar aggregates for d = 3, χ = 0.20, and ρ = 0.005.

DOI: 10.1021/acs.jpcb.9b08617
J. Phys. Chem. B 2019, 123, 9272−9280

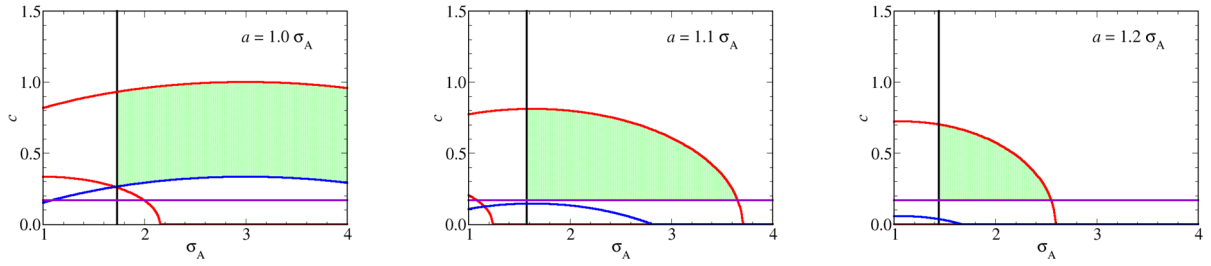

Figure 12. Graphical solution of eqs 5−7. For each a considered, the allowed values of σ_A and c fall within the green region. Both σ_A and c are given in units of σ_{B_2}.

must satisfy the condition $\sigma_{AB_1} \le r \le \sigma_{AB_1} + \sigma_{B_1}$, that is, $2/3 \le r \le 1$, which indeed is met by $r = \sqrt{3}/2$.

Clearly, thermal fluctuations impose an effective nearest-neighbor distance (b) that is not exactly equal to 1. We may ask how much a and b can be scaled up relative to their limiting values, so that we still have six A−B_1 bonds per sphere. Hence, for a generic value of σ_A, we take $a = \sqrt{2}(1 + \delta)\sigma_A$, $b = (1 + \delta)\sigma_A$, and $c = a/2$, where $\delta > 0$ is the relative increment of distances due to fluctuations. Binding is guaranteed if $\sigma_{AB_1} \le \sqrt{a^2 + b^2}/2 \le \sigma_{AB_1} + 1/3$, or

$$\sigma_{min} \equiv \frac{1}{3\sqrt{3} - 3 + \delta} \le \sigma_A \le \sigma_{max} \equiv \frac{1}{\sqrt{3}(1 + \delta) - 1} \tag{4}$$

Whereas σ_{min} is less than 1, σ_{max} is a decreasing function of δ that assumes a value of 1.366 for $\delta = 0$. Hence we conclude that no crystalline bilayer of the kind observed for $d = 1$ can exist for $d = 2$ or 3. Looking at $g_{AA}(r)$ for $\sigma_A = 1$ (Figure 8, bottom), we see a first-neighbor peak at 1 (corresponding to the minimum value of b or, equivalently, d_{ss}), a second-neighbor maximum at ∼1.49 (corresponding to a), and a third-neighbor maximum at ∼1.83 (corresponding to $\sqrt{a^2 + b^2}$). From the value of a we get $\delta = 0.054$, which gives $b = 1.054$ and $\sqrt{a^2 + b^2} = 1.825$, as indeed observed.

3.3.2. Triangular Sheet. We now consider a triangular carpet of spheres with spacing $a \ge \sigma_A$. Dimers are located in correspondence of the interstices of the sphere crystal, on both sides of it, and are perpendicularly oriented. In a convenient reference frame, the coordinates of three neighboring spheres are $(0, 0, 0)$, $(a, 0, 0)$, and $(a/2, a\sqrt{3}/2, 0)$. With c defined as the distance of a B_1 monomer from the plane of spheres, the coordinates of the B_1 and B_2 particles that are equidistant from the three spheres are, on the upper side of the plane, $(a/2, a\sqrt{3}/6, c)$ and $(a/2, a\sqrt{3}/6, c + 2/3)$. Taking into account the B_1 monomer that is placed symmetrically below the plane of spheres, the smallest c allowed is $\sigma_{B_1}/2 = \sigma_{B_2}/6$. In order for A and B_1 particles to be bound, it is necessary that

$$\frac{\sigma_A + 1/3}{2} \le \sqrt{\frac{a^2}{3} + c^2} \le \frac{\sigma_A + 1/3}{2} + \frac{1}{3} \tag{5}$$

To prevent overlap between spheres and B_2 monomers, the condition is

$$\sqrt{\frac{a^2}{3} + \left(c + \frac{2}{3}\right)^2} \ge \frac{\sigma_A + 1}{2} \tag{6}$$

Finally, we require that

$$a\frac{\sqrt{3}}{3} \ge \sigma_{B_2} = 1 \tag{7}$$

to rule out the possibility of lateral overlap between B_2 monomers. The value of a is not exactly known, but from a glance at many snapshots, we expect that its typical value is only slightly larger than σ_A. In Figure 12 we analyze three cases (from left to right, $a/\sigma_A = 1$, 1.1, and 1.2): eq 5 is satisfied for c values within the two red lines; eq 6 is satisfied for c values above the blue line; eq 7 is satisfied for σ_A values falling on the right of the vertical black line; and finally, $c \ge 1/6$ holds above the purple line. All in all, the only σ_A and c values consistent with the existence of (flat, infinite) triangular membranes are those within the green regions in Figure 12. As a/σ_A increases, the range of $d = \sigma_A/\sigma_{B_2}$ where membranes exist gets reduced; in all three cases considered, $d = 1$ is never allowed.

4. CONCLUSIONS

We have found rich self-assembly behavior in a colloidal mixture of spheres and dimers with only a few basic assumptions about the interaction governing particle aggregation. Upon variation of the sphere size and the relative concentration of the species, our system spontaneously gives rise to as many diverse aggregates as micelles, gel-like networks, bilayers, crystalline membranes, and vesicles, providing further proof of the stunning simplicity of the mechanism behind many complex structures also present in nature. Since colloidal particles with characteristics similar to those envisaged in the present model can actually be engineered, e.g., with the method explained in ref 18, our results may readily find application in various fields, such as encapsulation technology or the development of novel mesoporous materials for heterogeneous catalysis. We are aware that the outcome of a simulation may in principle depend on the kinetics imposed by the algorithm chosen. This means that any discrepancy between the simulation dynamics and an experimental realization of the model on the colloidal scale could lead to differences in the self-assembly products. For example, MC simulations with local moves only can have problems with equilibrating clustering systems. The use of cluster moves may alleviate this problem (see, e.g., ref 41). In this regard, we observe that the use of a smart technique such as the aggregation-volume-bias algorithm does not change the self-assembly behavior of our system in any respect.[17] In the near future, we plan to carry out a more refined exploration of the parameter space of the model with the aim of characterizing the boundaries between the various self-assembled structures and the mechanisms of crossover between them.

DOI: 10.1021/acs.jpcb.9b08617
J. Phys. Chem. B 2019, 123, 9272−9280

AUTHOR INFORMATION

Corresponding Author

*E-mail: sprestipino@unime.it.

ORCID

Santi Prestipino: 0000-0002-6266-7025

Notes

The authors declare no competing financial interest.

ACKNOWLEDGMENTS

We dedicate this paper to the memory of our collaborator and dear friend Mimmo Gazzillo, theoretical physicist at Ca' Foscari in Venice, who unexpectedly passed away last year at age 68. This work was done using computer facilities made available by the PO-FESR 2007-2013 Project MedNETNA (Mediterranean Network for Emerging Nanomaterials).

REFERENCES

(1) Bianchi, E.; Capone, B.; Coluzza, I.; Rovigatti, L.; van Oostrum, P. D. J. Limiting the Valence: Advancements and New Perspectives on Patchy Colloids, Soft Functionalized Nanoparticles and Biomolecules. *Phys. Chem. Chem. Phys.* **2017**, *19*, 19847−19868.

(2) Kern, N.; Frenkel, D. Fluid-Fluid Coexistence in Colloidal Systems with Short-Ranged Strongly Directional Attraction. *J. Chem. Phys.* **2003**, *118*, 9882−9889.

(3) Zhang, Z.; Glotzer, S. C. Self-Assembly of Patchy Particles. *Nano Lett.* **2004**, *4*, 1407−1413.

(4) Russo, J.; Tartaglia, P.; Sciortino, F. Reversible Gels of Patchy Particles: Role of the Valence. *J. Chem. Phys.* **2009**, *131*, 014504.

(5) Munaò, G.; Preisler, Z.; Vissers, T.; Smallenburg, F.; Sciortino, F. Cluster Formation in One-Patch Colloids: Low Coverage Results. *Soft Matter* **2013**, *9*, 2652−2661.

(6) Fechete, I.; Vedrine, J. C. Nanoporous Materials as New Engineered Catalysts for the Synthesis of Green Fuels. *Molecules* **2015**, *20*, 5638−5666.

(7) Sciortino, F.; Giacometti, A.; Pastore, G. Phase Diagram of Janus Particles. *Phys. Rev. Lett.* **2009**, *103*, 237801.

(8) Holmberg, K.; Jönsson, B.; Kronberg, B.; Lindman, B. *Surfactants and Polymers in Aqueous Solution*; Wiley: Chichester, U.K., 2002.

(9) Yoon, J.; Knobler, C. B.; Maverick, E. F.; Cram, D. J. Dissymmetric New Hemicarcerands Containing Four Bridges of Different Lengths. *Chem. Commun.* **1997**, 1303−1304.

(10) Tang, Q.; Denton, A. R. Ion Density Deviations in Semipermeable Ionic Microcapsules. *Phys. Chem. Chem. Phys.* **2015**, *17*, 11070−11076.

(11) Munaò, G.; Costa, D.; Prestipino, S.; Caccamo, C. Encapsulation of Spherical Nanoparticles by Colloidal Dimers. *Phys. Chem. Chem. Phys.* **2016**, *18*, 24922−24930.

(12) Zhang, L.; Eisenberg, A. Multiple Morphologies of "Crew-Cut" Aggregates of Polystyrene-b-poly(acrylic acid) Block Copolymers. *Science* **1995**, *268*, 1728−1731.

(13) Israelachvili, J. N.; Mitchell, D. J.; Ninham, B. W. Theory of Self-Assembly of Hydrocarbon Amphiphiles into Micelles and Bilayers. *J. Chem. Soc., Faraday Trans. 2* **1976**, *72*, 1525−1568.

(14) Damasceno, P. F.; Engel, M.; Glotzer, S. C. Predictive Self-Assembly of Polyhedra into Complex Structures. *Science* **2012**, *337*, 453−457.

(15) Engel, M.; Damasceno, P. F.; Phillips, C. L.; Glotzer, S. C. Computational Self-Assembly of a One-Component Icosahedral Quasicrystal. *Nat. Mater.* **2015**, *14*, 109−116.

(16) Munaò, G.; Costa, D.; Prestipino, S.; Caccamo, C. Aggregation of Colloidal Spheres Mediated by Janus Dimers: A Monte Carlo Study. *Colloids Surf., A* **2017**, *532*, 397−404.

(17) Prestipino, S.; Munaò, G.; Costa, D.; Caccamo, C. Self-Assembly in a Model Colloidal Mixture of Dimers and Spherical Particles. *J. Chem. Phys.* **2017**, *146*, 084902.

(18) Wolters, J. R.; Verweij, E.; Avvisati, G.; Dijkstra, M.; Kegel, W. K. Depletion-Induced Encapsulation by Dumbbell-Shaped Patchy Colloids Stabilize Microspheres against Aggregation. *Langmuir* **2017**, *33*, 3270−3280.

(19) Hoshen, J.; Kopelman, R. Percolation and Cluster Distribution. I. Cluster Multiple Labeling Technique and Critical Concentration Algorithm. *Phys. Rev. B* **1976**, *14*, 3438−3445.

(20) Chen, I. A.; Walde, P. From Self-Assembled Vesicles to Protocells. *Cold Spring Harbor Perspect. Biol.* **2010**, *2*, a002170.

(21) Bernardes, A. Monte Carlo Simulation of Vesicle Self-Organisation. *J. Phys. II* **1996**, *6*, 169−174.

(22) Noguchi, H.; Takasu, M. Fusion Pathways of Vesicles: A Brownian Dynamics Simulation. *J. Chem. Phys.* **2001**, *115*, 9547−9551.

(23) Yamamoto, S.; Maruyama, Y.; Hyodo, S. Dissipative Particle Dynamics Study of Spontaneous Vesicle Formation of Amphiphilic Molecules. *J. Chem. Phys.* **2002**, *116*, 5842−5849; Erratum: *J. Chem. Phys.* **2002**, *117*, 2990.

(24) Cooke, I. R.; Kremer, K.; Deserno, M. Tunable Generic Model for Fluid Bilayer Membranes. *Phys. Rev. E* **2005**, *72*, 011506.

(25) Lenz, O.; Schmid, F. A Simple Computer Model for Liquid Lipid Bilayers. *J. Mol. Liq.* **2005**, *117*, 147−152.

(26) Noguchi, H.; Gompper, G. Dynamics of Vesicle Self-Assembly and Dissolution. *J. Chem. Phys.* **2006**, *125*, 164908.

(27) Weiss, T. M.; Narayanan, T.; Wolf, C.; Gradzielski, M.; Panine, P.; Finet, S.; Helsby, W. I. Dynamics of the Self-Assembly of Unilamellar Vesicles. *Phys. Rev. Lett.* **2005**, *94*, 038303.

(28) Fromherz, P. Lipid-Vesicle Structure: Size Control by Edge-Active Agents. *Chem. Phys. Lett.* **1983**, *94*, 259−266.

(29) For example, see: Noguchi, H. Cup-to-Vesicle Transition of a Fluid Membrane with Spontaneous Curvature. *J. Chem. Phys.* **2019**, *151*, 094903.

(30) Huang, C.; Quinn, D.; Sadovsky, Y.; Suresh, S.; Hsia, K. J. Formation and Size Distribution of Self-Assembled Vesicles. *Proc. Natl. Acad. Sci. U. S. A.* **2017**, *114*, 2910−2915.

(31) Nelson, D. R.; Peliti, L. Fluctuations in Membranes with Crystalline and Hexatic Order. *J. Phys. (Paris)* **1987**, *48*, 1085−1092.

(32) Seung, H. S.; Nelson, D. R. Defects in Flexible Membranes with Crystalline Order. *Phys. Rev. A: At., Mol., Opt. Phys.* **1988**, *38*, 1005−1018.

(33) Lidmar, J.; Mirny, L.; Nelson, D. R. Virus Shapes and Buckling Transitions in Spherical Shells. *Phys. Rev. E: Stat. Phys., Plasmas, Fluids, Relat. Interdiscip. Top.* **2003**, *68*, 051910.

(34) Kohyama, T.; Gompper, G. Defect Scars on Flexible Surfaces with Crystalline Order. *Phys. Rev. Lett.* **2007**, *98*, 198101.

(35) Haselwandter, C. A.; Phillips, R. Elastic Energy of Polyhedral Bilayer Vesicles. *Phys. Rev. E* **2011**, *83*, 061901.

(36) Bowick, M. J.; Sknepnek, R. Pathways to Faceting of Vesicles. *Soft Matter* **2013**, *9*, 8088−8095.

(37) Prestipino Giarritta, S.; Ferrario, M.; Giaquinta, P. V. Statistical Geometry of Hard Particles on a Sphere. *Phys. A* **1992**, *187*, 456−474.

(38) Prestipino Giarritta, S.; Ferrario, M.; Giaquinta, P. V. Statistical Geometry of Hard Particles on a Sphere: Analysis of Defects at High Density. *Phys. A* **1993**, *201*, 649−665.

(39) Wales, D. J.; Ulker, S. Structure and Dynamics of Spherical Crystals Characterized for the Thomson Problem. *Phys. Rev. B: Condens. Matter Mater. Phys.* **2006**, *74*, 212101.

(40) Guerra, R. E.; Kelleher, C. P.; Hollingsworth, A. D.; Chaikin, P. M. Freezing on a Sphere. *Nature* **2018**, *554*, 346−350; Addendum: *Nature* **2018**, *560*, E25.

(41) Whitelam, S.; Geissler, P. L. Avoiding Unphysical Kinetic Traps in Monte Carlo Simulations of Strongly Attractive Particles. *J. Chem. Phys.* **2007**, *127*, 154101.

DOI: 10.1021/acs.jpcb.9b08617
J. Phys. Chem. B 2019, 123, 9272−9280